Commun. Math. Phys. 83, 517–535 (1982)

Communications in Mathematical Physics

The Evolution of a Turbulent Vortex*

Alexandre Joel Chorin

Department of Mathematics, University of California, Berkeley, CA 94720, USA

Abstract. We examine numerically the evolution of a perturbed vortex in a periodic box. The fluid is inviscid. We find that the vorticity blows up. The support of the L_2 norm of the vorticity converges to a set of Hausdorff dimension ~ 2.5. The distribution of the vorticity seems to converge to a lognormal distribution. We do not observe a convergence of the higher statistics towards universal statistics, but do observe a strong temporal intermittency.

1. Introduction

We consider a straight line vortex imbedded in a three-dimensional periodic domain. We perturb the vortex and follow its evolution by a vortex method, in the hope that the calculation will shed light on aspects of the dynamics of vorticity which are significant for the understanding of turbulence.

The equations of motion are Euler's equations. The reasons for assuming that the viscosity is absent are spelled out in [3, 8]: It is reasonable and consistent with both numerical experience and available theory to assume that in a periodic domain the solution of the Navier-Stokes equations converge to the solution of the Euler equations strongly enough for the properties of the energy-containing and inertial ranges to be analyzable in the inviscid case. Such an assumption is implicitly made in Kolmogorov's theory of the inertial range.

The calculations can of course be pursued only for a short time, until the complexity of the flow outstrips the available computer memory and time. However, significant information can be gleaned in this short time. Long time calculations require a rescaling or a renormalization group procedure [8, 22, 29, 30].

* This work was supported in part by the Director, Office of Energy Research, Office of Basic Energy Sciences, Engineering, Mathematical and Geosciences Division of the U.S. Department of Energy, under contract W-7404-ENG-48, and in part by the Office of Naval Research, under contract N00014-76-C-0316

0010-3616/82/0083/0517/$03.80

We obtain numerical results consistent with the conclusion reached in [8, 27] that the L_1 and L_2 norms of the vorticity become infinite in a finite time. We confirm the conclusion, reached in [8] by a rescaling procedure, that the L_2 support of the vorticity shrinks to an object of Hausdorff dimension ~ 2.5, as predicted by Mandelbrot [23, 24]. Graphical representations of the solution display the complexity of the flow and provide an intuitive explanation for the occurrence of strange sets.

The vortex motion presents an interesting mixture of coherence and disorder. Universal statistics are not achieved in our calculation, and support is found for the coherent structure model of the inertial range [3, 6]. The distribution of vorticity is seen to be approximately lognormal, in a sense different from both the Saffman model [28] and Kolmogorov's assumption [17]. A striking temporal intermittency is observed, somewhat similar to a phenomenon observed by Siggia [29].

In summary, the vorticity stretches wildly but the constraint of energy conservation prevents it from spreading evenly and forces it into tight knots. In general, the amount of disorder in a turbulent flow is presumably a function of the available energy.

2. The Equations of Motion and their Approximate Solution

The general framework for our calculation is similar to the one in [8]. The Euler equations for incompressible inviscid flow can be written in the form

$$\partial_t \boldsymbol{\xi} + (\mathbf{u} \cdot \nabla)\boldsymbol{\xi} - (\boldsymbol{\xi} \cdot \nabla)\mathbf{u} = 0, \tag{1a}$$

$$\boldsymbol{\xi} = \operatorname{curl} \mathbf{u}, \quad \operatorname{div} \mathbf{u} = 0, \tag{1b, c}$$

where $\mathbf{u}$ is the velocity, $\boldsymbol{\xi}$ is the vorticity, t is the time, and ∇ is the differentiation vector. These equations are to be solved in a box of side 1, with periodic boundary conditions.

Suppose the initial data can be approximated by M vortex tubes of small but finite cross-section. The circulation of the i^{th} tube is Γ_i. Let $\mathbf{r}(t)$ be the radius vector of a point moving with the fluid. The velocity induced by the tubes at $\mathbf{r}(t)$, as determined by Euler's equation, can be approximated by the Biot-Savart law (see [1]):

$$\mathbf{u}(\mathbf{r}) = -\frac{1}{4\pi} \sum_{i=1}^{M} \Gamma_i \int_{\substack{i^{\text{th}} \\ \text{tube}}} \frac{\mathbf{a} \times d\mathbf{s}}{a^3}, \tag{2}$$

where $\mathbf{s} = \mathbf{s}(\mathbf{r}')$ is the unit tangent to the i^{th} tube at $\mathbf{r}'$, ds is the element of arc length along that axis, $d\mathbf{s} = \mathbf{s}\, ds$, $\mathbf{a} = \mathbf{r} - \mathbf{r}'$, and $a = |\mathbf{a}|$ is the length of $\mathbf{a}$. If $\mathbf{r}$ lies on one of the tubes, formula (2) has to be modified and the finite cross-section taken into account, because a can vanish and the velocity induced by close-neighbor interaction on infinitely thin tubes is, in general, infinite (see, e.g., [1]). Thus, if $\mathbf{r}(t)$ is a point on the axis of one of the tubes, its velocity is given approximately by

$$\mathbf{u}(\mathbf{r}) = -\frac{1}{4\pi} \sum_{i=1}^{M} \Gamma_i \int_{\substack{i^{\text{th}} \\ \text{tube}}} \frac{\mathbf{a} \times d\mathbf{s}}{\psi(a)}, \tag{3}$$

where $\psi(a) = a^3$ when a is large, and $\psi(a)$ satisfies, among other constraints, the condition

$$\lim_{\delta \to 0} \int_{\mathbf{r}-\mathbf{s}\delta}^{\mathbf{r}+\mathbf{s}\delta} \frac{\mathbf{a} \times d\mathbf{s}}{\psi(a)} = 0.$$

The motion of $\mathbf{r}$ is then given by

$$\frac{d\mathbf{r}}{dt} = \mathbf{u}(\mathbf{r}). \tag{4}$$

Equation (3) is our point of departure for approximating Eqs. (1). We assume that the initial data are such that the initial vorticity can be approximated by N vortex segments, i.e., short, thin, circular cylinders whose axis is tangent at a point to the vorticity vector (Fig. 1). The coordinates of the center of the base of the i^{th} segment

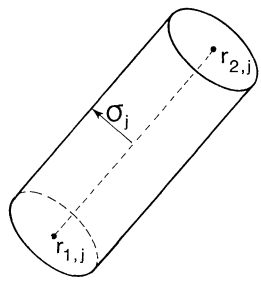

Fig. 1. A vortex segment

are $\mathbf{r}_i^{(1)} = (x_i^{(1)}, y_i^{(1)}, z_i^{(1)})$, and the coordinates of the center of the top are $\mathbf{r}_i^{(2)} = (x_i^{(2)}, y_i^{(2)}, z_i^{(2)})$. The i^{th} segment has a "circulation" Γ_i,

$$\Gamma_i = \int_{\substack{\text{cross} \\ \text{section}}} \boldsymbol{\xi} \cdot \mathbf{d\Sigma}$$

and radius σ_i, $i = 1, \ldots, N$. Connected segments remain connected, $\mathbf{r}_i^{(2)} = \mathbf{r}_{i+1}^{(1)}$. (For another example of the use of such segments, see [7]; in the present inviscid calculation, the difference between an algorithm based on the use of segments and the filament algorithm of [8] is merely one of book keeping.) No segment is allowed to be longer than a predetermined small number h, $|\mathbf{r}_i^{(2)} - \mathbf{r}_i^{(1)}| \leqq h$ for all i.

The vectors $\mathbf{r}_i^{(1)}$, $\mathbf{r}_i^{(2)}$ move according to an approximation of Eq. (4):

$$\begin{aligned}
&\mathbf{r}_i^{(1)n} \equiv \mathbf{r}_i^{(1)}(nk),\ \mathbf{r}_i^{(2)n} \equiv \mathbf{r}_i^{(2)}(nk),\ n \text{ integer},\ k = \text{time step};\\
&\mathbf{r}_i^{(1)n+1} = \mathbf{r}_i^{(1)n} + k\mathbf{u}_i^{(1)},\\
&\mathbf{u}_i^{(1)} = -\frac{1}{4\pi} \sum_{j=1}^{N} \Gamma_j \frac{\mathbf{a} \times \Delta\mathbf{r}_j}{\phi(a)},\\
&\Delta\mathbf{r}_j = \mathbf{r}_j^{(2)} - \mathbf{r}_j^{(1)},\\
&\mathbf{a} = \tfrac{1}{2}(\mathbf{r}_j^{(2)} + \mathbf{r}_j^{(1)}) - \mathbf{r}_i^{(1)},\\
&a = |\mathbf{a}|;
\end{aligned} \tag{5}$$

with similar expressions for $\mathbf{r}_i^{(2)n+1}$. We choose the following form of ϕ [which corresponds to ψ in (3)]:

$$\frac{1}{\phi(a)} = \begin{cases} (a_{\min}^2 a)^{-1} & \text{if } a \leqq a_{\min}, \\ a^{-3} & \text{if } a_{\min} \leqq a \leqq a_{\max}, \\ 0 & \text{if } a > a_{\max}, \end{cases}$$

$a_{\min}$, $a_{\max}$ are parameters to be chosen. The assumption $1/\phi = 0$ if $a > a_{\max}$ is convenient, and is reasonable since $1/\phi$ is small when a is large. If the vortex tubes are closed, there is no need to compute both $r_i^{(1)n+1}$ and $r_i^{(2)n+1}$. The time step k is chosen by requiring that

$$\max_i |\mathbf{r}_i^{(1)n+1} - \mathbf{r}_i^{(1)n}| = k \max |\mathbf{u}_i^{(1)n}| \leqq K, \quad K = \text{small constant}. \tag{6}$$

There are thus four parameters: $a_{\min}$, $a_{\max}$, h and K to be chosen; this will be done in the next section. Note that in a periodic box each vortex element interacts not only with each other segment but also with an infinite set of images of that other segment; however, if $a_{\max} < \frac{1}{2}$ only one of these interactions is non-zero.

Note also that the function ϕ is independent of the curvature of the vortex tubes. Numerical methods with such geometry-independent cut-off functions ϕ have been tested, e.g., in [7, 8], and have been shown to converge in [2]. On the other hand, it is known that for a single vortex line the leading term in an asymptotic expansion of its induced velocity field is curvature-dependent (see, e.g., [1, 14, 19]). The paradox is resolved by the fact that a single physical vortex may have to be approximated by a cloud of vortex segments, whose collective motion resolves all effects, including local curvature effects. A similar situation holds for vortex motion in the plane, where clouds of non-deformable numerical vortex elements approximate well the motion of deformable physical vortices [13]. Furthermore, I have run three-dimensional calculations in which every vortex was moved only by its local curvature-dependent self-induction, following Hama [14]. The resulting motion turned out to be slow and the vortex stretching insignificant. This suggests that even though the self-induction curvature-dependent term may be large for a single vortex with an arbitrarily chosen geometry, in its natural motion a vortex rearranges itself so that the self-induction effect is lessened.

We shall assume that the vortex segments retain a cylindrical cross-section throughout their evolution, in the expectation that an arbitrary vorticity configuration can be approximated by cylindrical segments. The theory in [2] and the analogy with the two-dimensional situation lend support to this expectation. Furthermore, we assume that the distribution of vorticity remains uniform within each segment. This assumption is not essential, but does simplify the bookkeeping.

As the flow evolves, the vortex segments stretch. If a segment becomes longer than h, it is broken up into two segments, each with half the original length. The new end-points are determined by linear interpolation. The cumulative stretching of the line is tracked as follows: Each segment $\overline{\mathbf{r}_i^{(1)}\mathbf{r}_i^{(2)}}$ is assigned a tag q_i. When the i^{th} segment is broken up into two halves, each one of the new segments is assigned a tag

equal to $2q_i$. Initially, $q_i = l_{0i}/V_i$, where V_i is the volume of the i^{th} segment and l_{0i} is its initial length. The number of segments, N, increases with time. In our calculations, we assumed that initially $V_i = V_0$ for all i; we also assumed that the segments had equal initial lengths $l_0 \leqq h$.

Let l_i be the length of the i^{th} segment, $l_i = |\mathbf{r}_i^{(2)} - \mathbf{r}_i^{(1)}|$, $|l_i| \leqq h$. The tag assigned to that segment had been doubled each time the length of a segment had been halved. The cross-section of the segment is thus $l_0/l_i q_i$, and its volume is l_0/q_i. Thus, the total volume occupied by the vortex segments is

$$V = l_0 \sum_{i=1}^{N} \frac{1}{q_i};$$

it is easy to see that V is constant in time with our computing scheme, as Eq. (1c) requires.

Assume that initially each vortex segment contains vorticity ξ, parallel to its axis, with $|\xi| = \xi_0$ equal for all segments. The L_1 norm of the vorticity, $\|\xi\|_1 = \int |\xi| \, dV$, can be evaluated as follows: Since the cross-section of the i^{th} segment is $l_0/l_i q_i$, the vorticity in the i^{th} segment is proportional to $l_i q_i$, and, therefore, up to an immaterial constant,

$$\|\xi\|_1 = \sum_{i=1}^{N} l_i . \tag{7}$$

By a similar argument, the L_2 norm of ξ equals

$$\|\xi\|_2^2 \equiv \int |\xi|^2 dV = \sum_{i=1}^{N} q_i l_i^2 , \tag{8}$$

where, again, an immaterial constant has been omitted. For simplicity, we shall henceforth omit factors such as l_0 when they play no role.

All the calculations below were made with the following initial data: A vertical cylindrical vortex is deformed in such a way that its axis consists of four straight lines through the points $(\frac{1}{2}, \frac{1}{2}, 0)$, $(\frac{1}{2}, \frac{1}{2}, \frac{2}{5})$, $(\frac{1}{2}, \frac{1}{2} + 0.1, \frac{3}{5})$, $(\frac{1}{2}, \frac{1}{2}, \frac{4}{5})$, $(\frac{1}{2}, \frac{1}{2}, 1)$. This vortex is then divided into segments of length smaller than h, and is assigned some cross-section S_0. $\Gamma_j = 1$ for all j.

Note that in [7] we set $\sigma_i = a_{\min}$ for all i. This identification was natural, but in no way logically required, and will not be used here.

3. Accuracy and Numerical Parameters

In the present section we show how the numerical parameters needed in our calculation are picked, and demonstrate that under suitable conditions the results obtained are independent of these parameters.

Consider first the dependence of the computed solution on the parameter K which determines the time step k. The behavior of the solution as a function of time is hard to use in assessing accuracy, since the velocity $\mathbf{u}$ increases very fast and a substantial part of the total time elapsed in 40 time steps is in fact spent in the first time step. Since the initial data are fixed, the length of the first step is proportional to K, and solutions with different K's appear as translates of each other in time. In

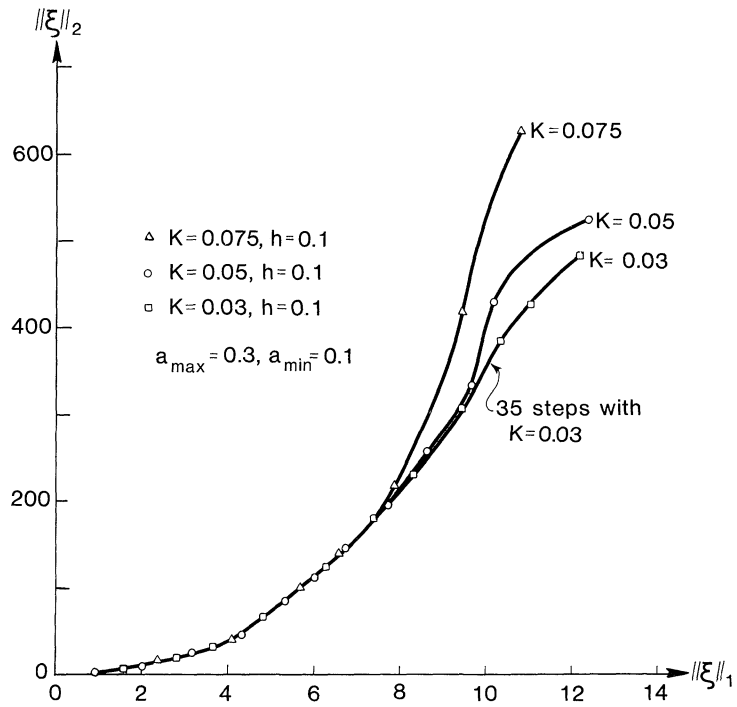

Fig. 2. (L_1, L_2) portrait of the calculations

order to remove this effect, we consider the (L_1, L_2) portrait of the flow, i.e., the curve traced by the flow in a plane where the coordinates are $\|\xi\|_1$ and $\|\xi\|_2$. From formulas (7), (8) it is seen that $\|\xi\|_2$ depends more on the total stretching than does $\|\xi\|_1$.

In Fig. 2 we display the (L_1, L_2) portraits of calculations performed with $a_{\min} = 0.1$, $a_{\max} = 0.3$, $h = 0.1$, and $K = 0.075$, 0.05, 0.03. One can see that as $K \to 0$ the curves converge to a limiting curve. A calculation with $K = 0.02$ is indistinguishable in this representation from the calculation with $K = 0.03$, for the times under consideration. When $a_{\min} = 0.1$, $a_{\max} = 0.3$, $h = 0.1$, we choose $K = 0.03$.

The runs made with $h = 0.075$ and $h = 0.05$ ($a_{\min} = 0.1$, $a_{\max} = 0.3$, $K = 0.03$) are indistinguishable in the (L_1, L_2) plane from the one made with $h = 0.1$. The runs made with $h = 0.1$, $K = 0.03$, $a_{\min} = 0.1$, and $a_{\max} = 0.2$, 0.3, 0.4, 0.5 are also indistinguishable.

However, if $a_{\min}$ is reduced, K and h have to be reduced also. When they are reduced substantially the calculation returns to the portrait it had with $a_{\min} = 0.1$. One can see that all that happens is that the time and space scales are reduced and the calculation merely rescaled. Thus, we shall pick in all the runs below $a_{\min} = 0.1$, $a_{\max} = 0.3$, $h = 0.1$, $K = 0.03$.

We also made some runs with $a_{\min}$ variable, and dependent on the local cross-section of the segments. With appropriate values of K, $a_{\max}$ and h the calculation gives the same results as the one with constant $a_{\min}$.

The lack of sensitivity of the results to parameters such as $a_{\min}$, $a_{\max}$ underscores, once again, the fact that some of the properties of turbulence are reasonably independent of the exact form of the equations of motion, a phenomenon already familiar from the theory of critical phenomena (see, e.g., [30]).

Another check on the accuracy of the calculation is the verification of energy conservation. The energy in the periodic box is

$$E = \tfrac{1}{2} \int |\mathbf{u}|^2 dV. \quad \mathbf{u} = \text{velocity vector}.$$

E should be approximately constant in time. $\mathbf{u}$ can be computed at an arbitrary point by an obvious extension of formulas (5). The flow is very complex (see below) and it is hopeless to try to evaluate E by classical quadrature. The best we can do is distribute some points evenly in the box, evaluate $|\mathbf{u}|^2$ at these points, and average; in Table 1 we display the results of two such calculations, with $K = 0.03$, $a_{\min} = 0.1$, $a_{\max} = 0.3$, $h = 0.1$, and with 5^3 and 9^3 sample points respectively. Energy does appear to be as constant as the method by which it is evaluated would allow. In Table 2 we display the results of a run made with $K = 0.1$ (a value which we already know is too large). Energy is not conserved.

Each one of the major calculations below has been checked to see how sensitive it was to a variation in the numerical parameters.

Table 1. Energy conservation, $K = 0.03$

Step	5^3 sample points	9^3 sample points
1	0.17	0.19
5	0.16	0.18
10	0.15	0.17
15	0.16	0.16
20	0.18	0.15
25	0.18	0.17
30	0.20	0.18

Table 2. Energy (non)conservation, $K = 0.1$. 9^3 sample points

Step	Energy
1	0.14
5	0.15
10	0.21
12	0.77
14	0.32
16	0.45

4. Main Features of the Flow

As soon as the flow begins, the vorticity begins to stretch, and the stretching is extraordinarily rapid. In Fig. 3 we plot the evolution of $\| \xi \|_1$ as a function of time. The graph is consistent with the conclusion in [8] that $\| \xi \|_1$ (and *a fortiori* $\| \xi \|_2$)

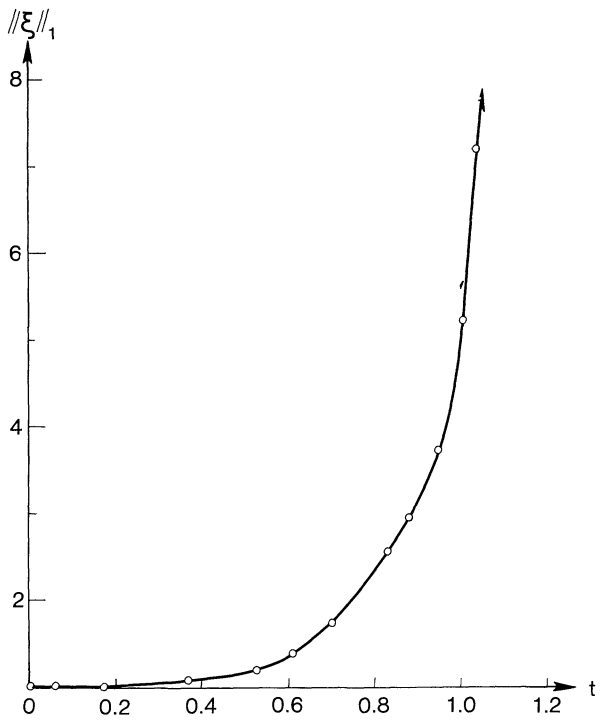

Fig. 3. $\|\xi\|_1$ as a function of time

become infinite in a finite time. Of course, as $\|\xi\|_1$ increases, the number of segments needed in the calculation increases, and the calculation cannot be continued forever.

Attach to each segment a stretching number $s_i = q_i l_i$, where q_i is the tag attached to the vortex segment and l_i is its length, $l_i = |\mathbf{r}_i^{(2)} - \mathbf{r}_i^{(1)}| \leqq h$. The length scale associated with each vortex is the square root of its cross-section; that scale is proportional to $1/\sqrt{s_i}$. By step 40, some segments have been stretched by a factor of ~ 400, while others have been stretched only by a factor of ~ 2. The ratio of the largest to the smallest scale at the end of step 40 is thus about 20 to 1. This is not a large enough spread to allow a determination of the inertial range exponent. We tried to calculate the average value of $(\mathbf{u}(\mathbf{x}+\mathbf{r}) - \mathbf{u}(\mathbf{x}))^2$, where $\mathbf{u}$ is the velocity and $r = |\mathbf{r}|$ is comparable with the scales present in the calculation, and then approximate this function by r^γ. The values of γ obtained in this way were not independent of the range of scales chosen, and ranged between 0.9 and 1.4.

As the flow evolves, $u_{\max} = \max_i |\mathbf{u}_i^{(1)}|$ increases rapidly even though the energy remains constant, and k, the time step, decreases from 0.37 at step 1 to 0.013 at step 40. An interesting interpretation of that fact is presented below.

In Fig. 4 we present the general configuration of the vortex segments after 10 steps ($t = 0.65$), 20 steps ($t = 0.88$), 30 steps ($t = 1.04$) and 40 steps ($t = 1.21$). The pattern of increasing complexity is obvious. However, the vortex does not forget the fact that its initial configuration was vertical (for a quantitative discussion, see

below). Some entrainment of irrotational fluid does take place, and can be measured as follows: Define the horizontal center of gravity of the vortex,

$$\bar{x}=\frac{1}{N}\sum_{i=1}^{N} x_i^{(1)}, \qquad \bar{y}=\frac{1}{N}\sum_{i=1}^{N} y_i^{(1)}.$$

The entrainment radius R is

$$R=\frac{1}{N}\sum_{i=1}^{N}\sqrt{(x_i^{(1)}-\bar{x})^2+(y_i^{(1)}-\bar{y})^2}. \tag{9}$$

R increases from $R=0.025$ at $t=0.37$ to $R=0.137$ at $t=1.17$.

The most remarkable feature of Fig. 4 is the fact that as the vortices stretch they organize themselves into coherent narrow sheaves. In Fig. 5 we show details of the structure at step 28, i.e., relatively early. At later times, the packing of the segments is so tight that it is difficult to discern in them a consistent pattern. (Indeed, one would not expect to have an intuitive grasp of an object of Hausdorff dimension ~ 2.5.) Some of the "legs" in Fig. 4d contain 20 to 30 separate segments.

The explanation for this phenomenon is as follows: As the vortices stretch, their cross-section decreases and the energy associated with them would increase unless they arranged themselves in such a way that their velocity fields cancelled. The folding achieves such cancellation; it will be reinterpreted in the next section in terms of Hausdorff dimension.

The large degree of coherence in the physical vortex cores, and the fact that stretching and folding rearrange the vorticity in thin, well-defined vortex structures, provide some support to the conjecture in [3, 6] that the inertial range spectrum is related to the spectral tail of the vorticity distribution in discrete vortex structures.

5. Hausdorff Dimension of the Support of Vorticity

In [8] we presented a calculation which verified Mandelbrot's conjecture that the L_2 support of the vorticity shrinks into a set of Hausdorff dimension ~ 2.5. The calculation in [8] was based on a rescaling argument whose validity is not rigorously established (for an example where rescaling has been applied and can be proved to be valid, see [9]). In the present section we obtain the same result by a different method.

We first define Hausdorff dimension. Consider a compact set C; cover it by a finite collection of balls of radii ϱ_i, $\varrho_i \leqq \varrho$. Form the sum

$$S(D)=\sum_i \varrho_i^D, \qquad D=\text{positive number}.$$

Consider the quantity

$$h(D)=\lim_{\varrho\to 0}\lim \inf S(D).$$

$h(D)$ is the Hausdorff measure of C in dimension D. $h(D)$ is zero for D large, usually infinite for D small; the number

$$D^*=\begin{cases}\text{greatest lower bound of } D \text{ for which } h(D) \text{ is zero,}\\ \text{smallest upper bound of } D \text{ for which } h(D) \text{ is infinite,}\end{cases}$$

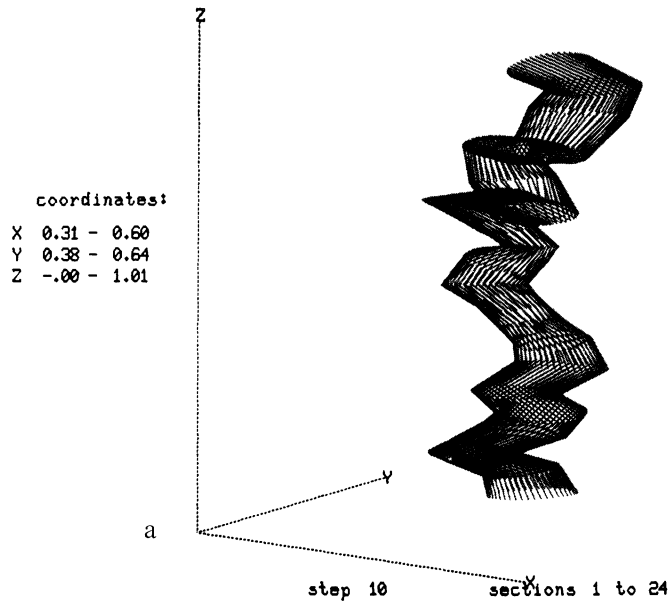

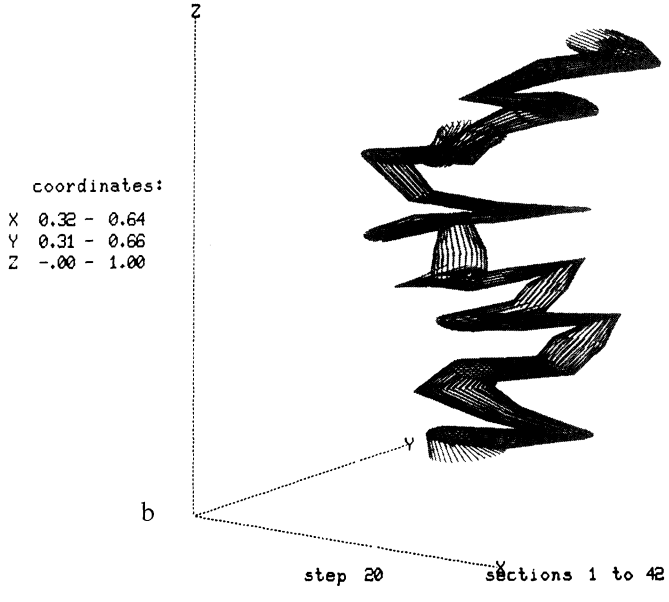

Fig. 4a–d. The evolution of the vortex: **a** step 10, time = 0.65 **b** step 20, time = 0.88

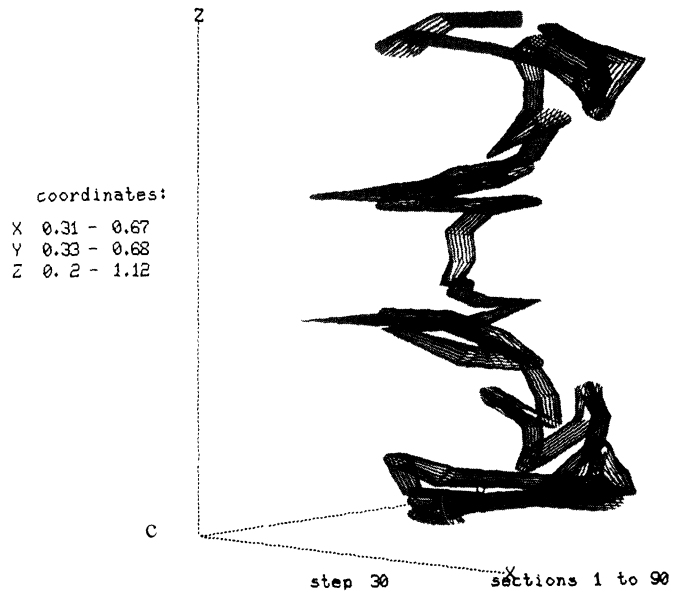

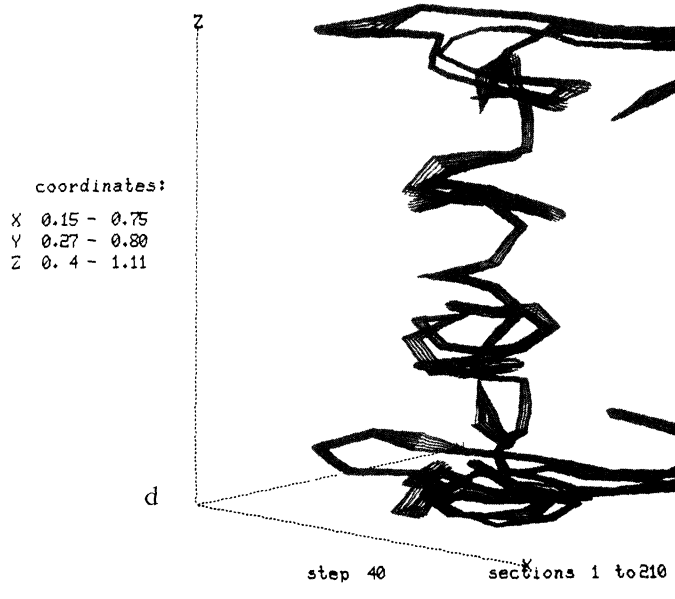

c step 30, time = 1.04 **d** step 40, time = 1.21

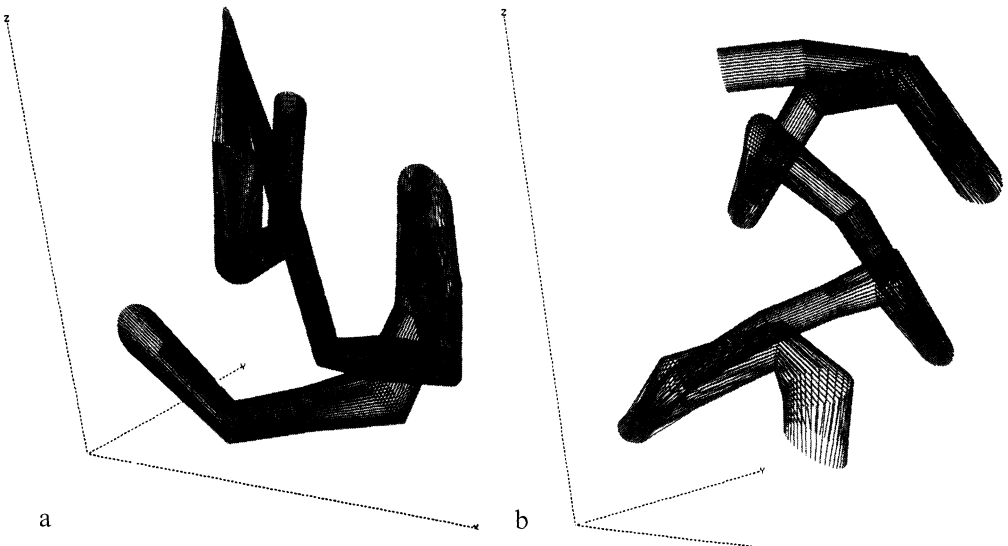

Fig. 5a and b. Two details of the flow, step 28

is the Hausdorff dimension of C. For a cube $D^* = 3$, for a square $D^* = 2$, for a line segment $D^* = 1$, for the tertiary Cantor set $D^* = \log 2/\log 3$ (see [16]). The balls used in the definition of D^* can be replaced by any family of non-degenerate self-similar objects [12].

The conjecture verified in [8] is the following: Consider $\|\xi\|_2^2 = \int |\xi|^2 dV$. Consider any $\varepsilon > 0$. There is a time T such that for $t > T$ $\xi = \xi_1 + \xi_2$, the supports of ξ_1 and ξ_2 are disjoint, the support of ξ_1 has dimension $D^* \cong 2.5$, and $\|\xi_1\|_2^2 = (1-\varepsilon)\|\xi\|_2^2$; i.e., almost all the vorticity has support of dimension D^*.

We verify this conjecture here by a different method. Consider the stretching numbers $s_i = l_i q_i$. We pick an ε, and determine $s^* = s^*(\varepsilon)$ such that

$$\sum_{\substack{\text{segments} \\ \text{such that} \\ s_i > s^*}} q_i l_i^2 = (1-\varepsilon) \sum_{\substack{\text{all} \\ \text{segments}}} q_i l_i^2,$$

[see formula (8)]. We cover the segments for which $s_i > s$ by cylinders with circular bases whose heights are equal to the radius ϱ_i of their bases. A segment of length l_i with tag q_i has cross-section $1/l_i q_i$ and can be covered by cylinders with $\varrho_i = 1/\sqrt{l_i q_i}$. The sum $S(D)$ which corresponds to this cover is

$$S(D) = \sum_{s_i > s^*} l_i \sqrt{l_i q_i} \left(\frac{1}{l_i q_i}\right)^{D/2}, \quad s^* = s^*(\varepsilon). \tag{10}$$

$S(D)$ approximates the lim inf of sums corresponding to covers with such cylinders. Indeed, consider one segment. A cover with smaller cylinders will only increase $S(D)$ (since when we double the number of cylinders we decrease the factor ϱ^D by less than two); on the other hand, if we cover the segment by larger cylinders of radii, say, α, there will be $\sim l_i/\alpha$ such cylinders and the corresponding contribution

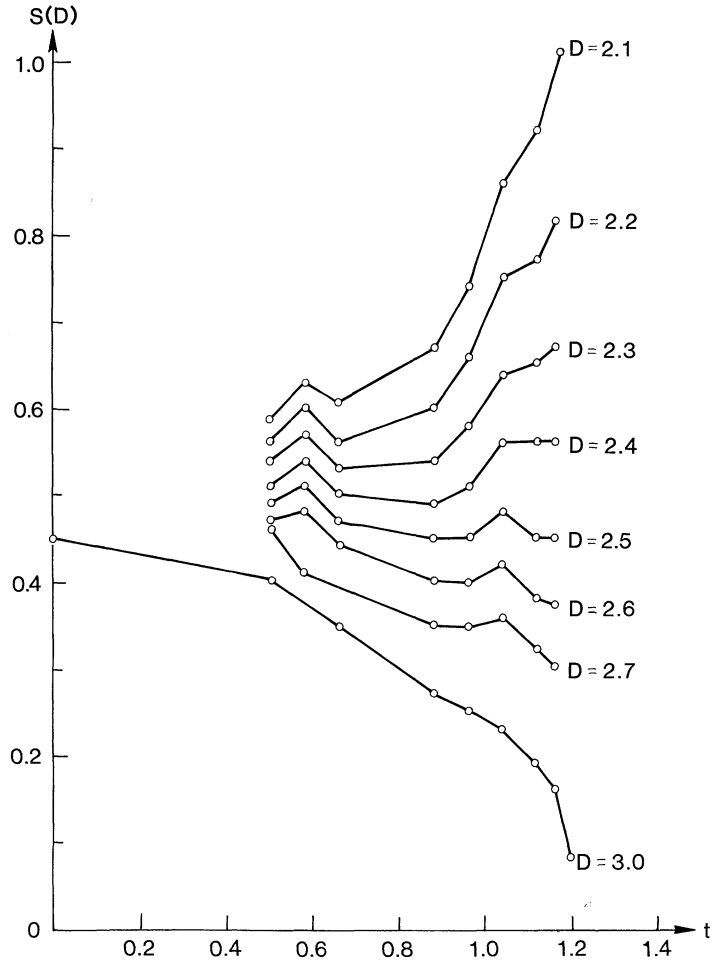

Fig. 6. Hausdorff sums as functions of time

to $S(D)$ will be $\sim (l_i/\alpha)\alpha^D = l_i \alpha^{D-1}$. If $D > 1$ (which will turn out to be the case in all the calculations below) the contribution to $S(D)$ is smallest when α is as small as possible. We follow the sums $S(D)$ in time, relying on the fact that the segments are stretching, and thus that the $1/\sqrt{l_i q_i}$ are decreasing, to produce the limit of vanishing linear dimension.

In Fig. 6 we plot the evolution of $S(D)$ for several values of D, with $\varepsilon = 0.1$. For small t, $S(D)$ is not always defined because there are not enough segments for s^* to be defined. Note that at $t = 1.21$, $S(3) = 0.08$; initially $S(3) = 0.45$; i.e., at $t = 1.21$, 90% of the squared vorticity is contributed by 16% of the volume originally occupied by vorticity. For $D < D^*$, $S(D)$ should be increasing; for $D > D^*$, $S(D)$ should be decreasing. An inspection of Fig. 6 leads to the estimate $D^* \sim 2.5$, in agreement with the conclusion of [8].

The notion of Hausdorff dimension provides an interpretation of the process of vortex folding described in the preceding section. The vorticity keeps on stretching and eventually, after a finite or infinite time has elapsed, some cross-section of a vortex line should have zero Lebesgue measure. However, that cross-section cannot shrink to a point because the energy associated with a point vortex is infinite. Sets of non-integer Hausdorff dimension appear in problems where, for example, one tries to characterize sets of zero Lebesgue measure which can carry a finite charge while giving rise to a bounded potential (see [12]). It seems likely that the constraint of finite energy requires that a cross-section of an infinitely stretched vortex have a sufficiently large Hausdorff dimension. The cross-section of a set of Hausdorff dimension $2+\alpha$ will in general have Hausdorff dimension $1+\alpha$ (see [26]). The process of vortex folding is the process by which such a cross-section is generated.

In [11], Frisch et al. presented an interesting derivation of the relationship between an energy cascade and Hausdorff dimension. They considered eddies of typical linear dimension L, containing energy proportional to βU^2, where β is the decreasing fraction of volume occupied by active eddies of linear dimension L. The characteristic time T of such eddies is $\sim L/U$, and the Kolmogorov assumption is that in a characteristic time T the eddies lose their energy to smaller eddies, the rate of energy transfer $\beta U^2/T = \beta U^3/L$ being constant. It is difficult to verify such assumptions on the computer, since quantities such as U, L and T are not sharply defined. However, consider the flow in the periodic cube as making up a single eddy. $\beta U^2 =$ constant, and if β is decreasing, U should increase, and it does. The quantity $\max_i |u_i|$ increases while $\int u^2\, dV$ remains constant because the activity is confined to an ever decreasing volume. Accuracy requires that the time step k be a small fraction of the characteristic time. The characteristic time. L/U, is decreasing, and thus k should decrease; we have seen that it does.

6. Lognormality of the Vorticity Distribution

As the vortex lines stretch, the range of values $s_i = q_i l_i$, $i = 1, \ldots, N$, assumed by the vorticity increases. It is of interest to determine the distribution of the s_i.

In [2], Saffman provided an argument to show that the distribution of values assumed by the vorticity is lognormal; he assumed that the local rate of stretching is proportional to the local vorticity multiplied by a random coefficient:

$$\frac{d\xi}{dt} = b(t)\,\xi. \tag{11}$$

By integration we find

$$\log(\xi(t)) - \log(\xi(0)) = \int_0^t b(t)\, dt,$$

and if the values of $b(t)$ for distinct values of t are reasonably independent, and if all the $\log \xi(0)$ are equal, it follows that the distribution of $\xi(t)$ is lognormal. Assumption (11) is reasonable for a short time, for indeed the more vorticity has been stretched in a neighborhood, the more vorticity is available to perform further stretching; the stretching also depends on the geometrical configuration of the

Table 3. Skewness and flatness of $\log s$

Step	Skewness	Flatness
1	0.40	1.16
5	0.77	2.17
10	0.74	2.22
15	0.54	2.43
20	0.34	2.59
25	−0.60	3.35
30	−0.29	2.39
35	−0.19	2.25
40	−0.19	2.81

vortex which can quite reasonably be viewed as random. However, once the vorticity has been stretched a lot, vorticity contributions generated in one part of the flow interact with vorticity contributions generated in another part of the flow, so that (11) is no longer a convincing model.

A different lognormality was assumed to hold in Kolmogorov's theory [17]. He assumed that the distribution of dissipation in disjoint, fixed small volumes is lognormal. The two lognormality assumptions are different, and, as shown in [18] and [23], probably incompatible. We have been able to verify neither.

However, if we consider the distribution of the s_i's obtained by our algorithm, we see that it does at least approximately converge to a lognormal distribution. In Table 3 we display the skewness and flatness of the distribution of the computed $\log s_i$ as functions of time. These quantities are defined as follows: Let α be a random variable, and let an overbar denote an average at a fixed time. $V(\alpha) = \overline{(\alpha - \bar{\alpha})^2}$ is the variance of α, $Z(\alpha) = \overline{(\alpha - \bar{\alpha})^3}/V(\alpha)^{3/2}$ is the (normalized) skewness of α, and $K(\alpha) = \overline{(\alpha - \bar{\alpha})^4}/(V(\alpha))^2$ is the flatness of α. For a gaussian variable α, $Z(\alpha) = 0$ and $K(\alpha) = 3$. The values of $Z(\log s)$ and $K(\log s)$ have an error of approximately ± 0.3 (as can be seen by making several runs with different numerical parameters) and are compatible with the conclusion that $\log s$ has a normal distribution. In Fig. 7 we display the distribution of $(\log s - \overline{\log s})/V(\log s)$

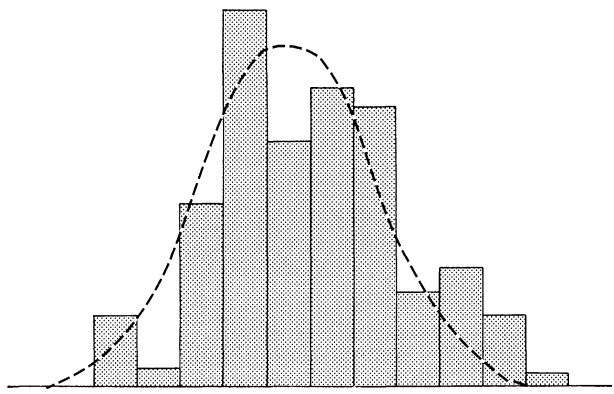

Fig. 7. Histogram of the vorticity distribution

as well as the gaussian distribution with the same mean and variance, after the 40th step. In view of the fairly small sample size, the assumption that $\log s$ is gaussian becomes quite tenable.

This conclusion agrees with Saffman's conjecture if the total amount of stretching is small, but differs from Saffman's conjecture when the stretching is substantial. Indeed, in our calculation each vortex is divided into shorter vortices when its length exceeds h, and each new piece contributes a value of $\log s$ when the statistics of $\log s$ are computed. On the other hand, in Saffman's model, each vortex contributes a single value however much it may have been stretched. Our distribution is therefore much less "intermittent" than Saffman's, and allows fewer extreme values of s. Our conclusion would agree with Kolmogorov's if the segments were equidistributed in space and if one could apply his conjecture to volumes which contain exactly one segment; the first condition is unlikely to hold (see Fig. 4) and the second condition is not compatible with the analysis in [17].

7. Temporal Intermittency and Higher Statistics

It has already been mentioned that during the short time interval for which our problem can be run, the flow does not forget its initial data; in particular, the velocity field remains on the whole the velocity field of a vertical vortex. Let $\mathbf{u} = (u, v, w)$ be the velocity vector. Quantities such as $\overline{u^2}$, $\overline{v^2}$, $\overline{w^2}$, where the overbar denotes spatial averages, can be computed by the sampling method described earlier for computing energy. At $t = 0$ $\overline{w^2} \sim 0$; $\overline{w^2}$ increases slowly (to about 20 % of $2E = \overline{u^2} + \overline{v^2} + \overline{w^2}$) and then starts to decrease again.

In Fig. 8 we display $\overline{u^2}$, $\overline{v^2}$, $\overline{w^2}$ averaged over the central subregion C_R: $\frac{1}{2} \pm R \leqq x \leqq \frac{1}{2} + R$, $\frac{1}{2} \pm R \leqq y \leqq \frac{1}{2} + R$, $0 \leqq z \leqq 1$, where R is the entrainment radius defined in Eq. (9). We picked that region because the fluid can be viewed as more fully turbulent there and one could have expected a closer approximation to energy equipartition between u, v, w in that region than in the cube as a whole. However, just the opposite is the case. $\overline{u^2}$ and $\overline{v^2}$ oscillate, as one would expect from the fact that the vortex as a whole precesses as a consequence of its initial perturbation; $\overline{w^2}$ increases sharply but then decreases sharply, leaving an almost two-dimensional flow. The graph of $\overline{w^2}$ contains a sharp blip.

It was interesting to see if a similar blip could be seen in any other statistical description of the flow. None could be seen in quantities such as the flatness or the skewness of the distribution of u or v (which remain roughly constant and merely reflect the fact that we have approximately a velocity field associated with a vertical vortex). We therefore tried to compute the skewness and flatness of velocity derivatives such as u_x.

u_x can be computed formally from (5) by differentiation:

$$u_x(\mathbf{r}) = C \sum_{j=1}^{N} (\mathbf{a} \times \Delta\mathbf{r}_j)_1 / \tilde{\phi},$$

where

$$\mathbf{a} = \tfrac{1}{2}(\mathbf{r}_j^{(2)} + \mathbf{r}_j^{(1)}) - \mathbf{r},$$

$$a = |\mathbf{a}|,$$

$$\Delta\mathbf{r}_j = \mathbf{r}_j^{(2)} - \mathbf{r}_j^{(1)}.$$

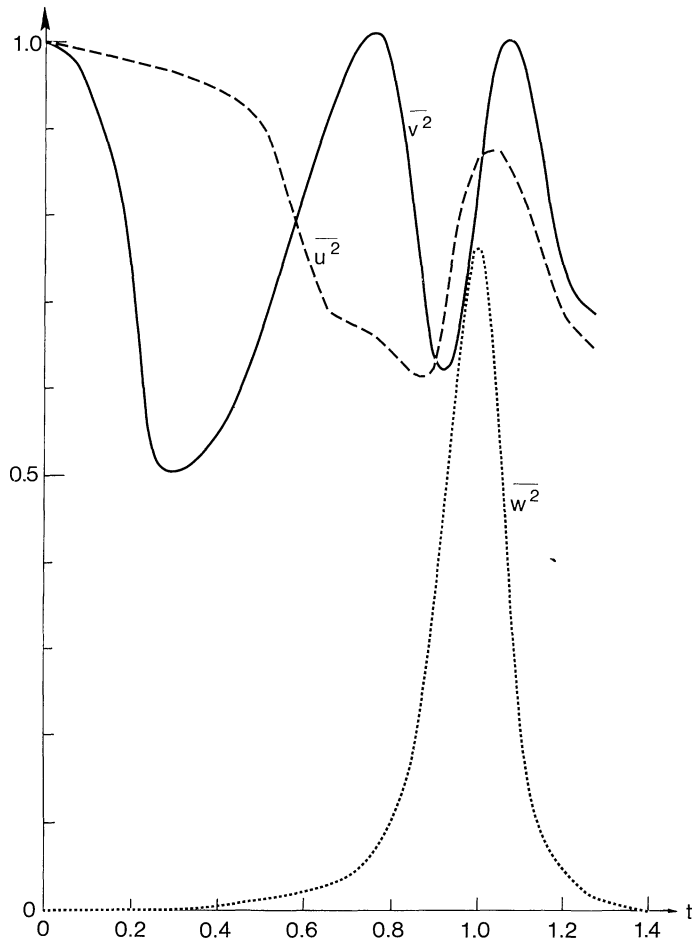

Fig. 8. $\overline{u^2}$, $\overline{v^2}$, $\overline{w^2}$ as function of time

$(\mathbf{a} \times \mathbf{r}_j)_1$ denotes the x component of $\mathbf{a} \times \Delta\mathbf{r}_j$, and

$$1/\tilde{\phi} = 1/\tilde{\phi}(a) = \begin{cases} a^{-2} a_{\min}^{-2} & \text{if} \quad a \leqq a_{\min} \\ a^{-4} & \text{if} \quad a_{\min} \leqq a \leqq a_{\max} \\ 0 & \text{if} \quad a > a_{\max}. \end{cases}$$

The constant C incorporates the factors $-1/4\pi$ and Γ_j of (5) as well as numerical coefficients which arise in the differentiation. It is not at all obvious that this differentiation leads to an approximation of u_x, and indeed the moments of u_x depend on $a_{\min}$, $a_{\max}$ as well as on the size of the region in which they are evaluated; only their qualitative behavior is of possible significance. The flatness of u_x exceeds the flatness of u for all choices of parameters.

It is not at all obvious either that the moments of u_x remain bounded in time (and indeed, we claimed earlier that $\|\xi\|_2$ did not remain bounded). Also, the theorem on equality of Hausdorff dimension and capacitory dimension [12]

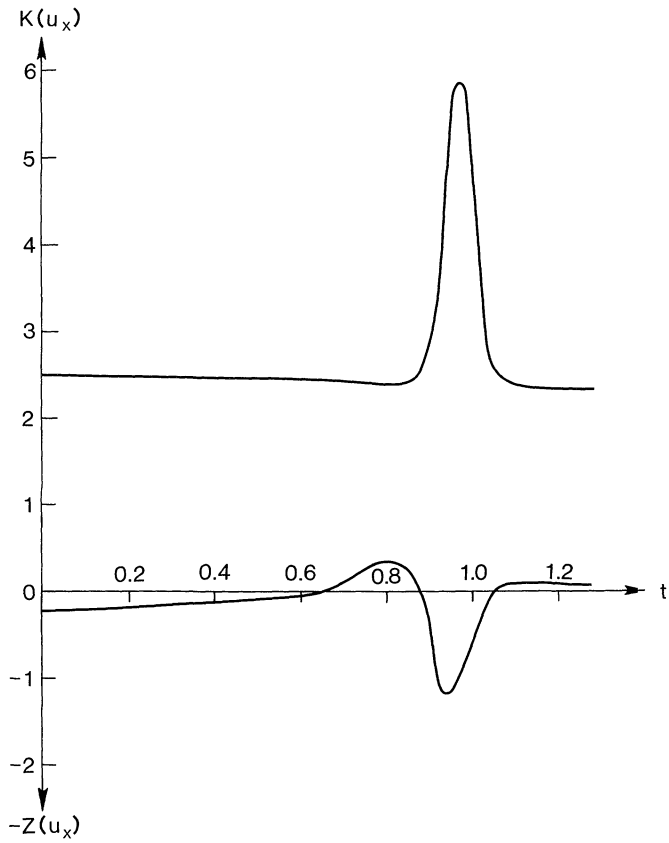

Fig. 9. Qualitative behavior of the skewness and flatmess of u_x

suggests that moments of sufficiently high derivatives of u do not exist, a conclusion reached by other means in [25]; this possibility casts a further doubt on the validity of the calculation of the moments of u_x.

Be that as it may, we have plotted in Fig. 9 the behavior of the skewness $Z(u_x)$ and flatness $K(u_x)$ of u_x averaged in space over the central region C_R. The temporal blip observed in the evolution of $\overline{w^2}$ has its clear equivalent here. Changes in the region over which the average is taken and in $a_{\min}$, $a_{\max}$ change the numerical values of S and K, but do not change the shape of the curve. The sudden increase in activity associated with the blip resembles the temporal intermittency observed by Siggia [29]. We have no good explanation for this phenomenon. It may be due to a vortex breakdown, such as the one observed numerically in [10], which could be responsible for the horizontal loops in Fig. 4d.

Note that nowhere in Figs. 8 and 9 do we observe a convergence towards statistics independent of the initial data. This may be due to the fact that the integration time is too short, but it could also be due to the non-existence of "universal" statistics. The experimental data (see, e.g., [31]) do not rule out the latter hypothesis. Arguments for and against the existence of "universal" statistics can be found e.g. in [25] and [29]. It seems likely that "universal" values of skewness

and flatness, if they exist, depend on temporal as well as spatial averaging. The calculation of β in [8] lends support to this conjecture.

8. Conclusion

We have provided quantitative and qualitative information about the evolution of a three-dimensional vortex, which has a substantial bearing on the assessment of various theoretical models of turbulent flow. Most importantly, we have demonstrated the eminent suitability of vortex methods for the analysis of turbulence. Long thin objects which arise in fluid turbulence are easier to represent as long thin objects than in any other way.

The calculations above were performed on a VAX computer at the Lawrence Berkeley Laboratory. Listings of the programs used are available from the author.

References

1. Batchelor, G.K.: An introduction to fluid mechanics. Cambridge: Cambridge University Press 1967
2. Beale, T., Majda, A.: Vortex methods: convergence in three dimensions. Math. Comp (to appear)
3. Chorin, A.J.: In Proc. 2d Int. Conf. Num. Meth. Fluid Mech., pp. 285–289 Berlin, Heidelberg, New York: Springer 1970
4. Chorin, A.J.: J. Fluid Mech. **57,** 785–796 (1973)
5. Chorin, A.J.: J. Fluid Mech. **63,** 21–32 (1974)
6. Chorin, A.J.: Lectures on turbulence theory. Boston: Publish/Perish 1975
7. Chorin, A.J.: SIAM J. Sc. Stat. Comp. **1,** 1–24 (1980)
8. Chorin, A.J.: Comm. Pure. Appl. Math. **34,** 853–866 (1981)
9. Chorin, A.J.: Numerical estimates of Hausdorff dimension. J. Comp. Phys. (to appear)
10. del Prete, V.: Numerical simulation of vortex breakdown. LBL Math. & Computing Report, Berkeley (1978)
11. Frisch, U., Salem, P.L., Nelkin, M.: J. Fluid Mech. **87,** 719–736 (1978)
12. Frostman, O.: Potentiel d'equilibre et capacité des ensembles. Thesis Lund (1935)
13. Hald, O.: SIAM J. Num. Anal. **10,** 726–755 (1979)
14. Hama, F.: Phys. Fluids **6,** 526–528 (1963)
15. Hausdorff, F.: Dimension und äußeres Maß. Math. Ann. **79,** 1 – 21 (1919)
16. Kahane, J.P., Salem, R.: Ensembles parfaits et séries trigonométriques. Paris: Hermann 1963
17. Kolmogorov, A.N.: J. Fluid Mech. **13,** 82–86 (1962)
18. Kraichnan, R.H.: J. Fluid Mech. **62,** 305–330 (1974)
19. Lamb, H.: Hydrodynamics. London: Dover 1960
20. Leonard, A.: Proc. 4th Int. Conf. Num. Meth. Fluid Mech., pp. 245–250. Berlin, Heidelberg, New York: Springer 1975
21. Leonard, A.: J. Comput. Phys. **37,** 289–335 (1980)
22. Ma, S.K.: Modern theory of critical phenomena. Reading: Benjamin, 1977
23. Mandelbrot, B.: In: Statistical models and turbulence, Rosenblatt, M., Van Atta, C. (eds.) pp. 333–358. Berlin, Heidelberg, New York: Springer 1972
24. Mandelbrot, B.: J. Fluid Mech. **62,** 331–358 (1974)
25. Mandelbrot, B.: In: Turbulence and NS equation, Temam, R. (ed.) pp. 121–145. Berlin, Heidelberg, New York: Springer 1976
26. Mattila, P.: Ann. Acad. Sci. Finn. **A,** 1 (1975)
27. Morf, R., Orszag, S., Frisch, U.: Phys. Rev. Lett. **44,** 572–575 (1980)
28. Saffman, P.: Phys. Fluids **13,** 2193–2194 (1970)
29. Siggia, E.: J. Fluid Mech. **107,** 375–406 (1981)
30. Salem, P.L., Fournier, J.D., Pouquet, A.: In: Dynamical critical phenomena and related topics, Enz, C. (ed.). Berlin, Heidelberg, New York: Springer 1979
31. Van Atta, C., Antonia, R.: Phys. Fluids **23,** 252–268 (1980)

Communicated by J. Glimm

Received September 25, 1981